









Cedar tar as a green corrosion inhibitor for E24 steel in 1 M HCl solution: A comparative analysis of uncleaned and cleaned cedar tar

O. Ninich,¹* E. El Fahime,² M. Tiskar,³ K. Tassaoui,⁴
O. Chauiyakh,¹ S. Aarabi,¹ B. Satrani,⁵ M. Benmessaoud⁴
and A. Ettahir¹

¹Materials, Energy, Acoustics Team, École Supérieure de Technologie - Salé, Mohammed V University, Rabat, Morocco

²National Center for Scientific and Technical Research, Rabat, Morocco

³Laboratory: Organic Chemistry, Catalysis and Environment. University Ibn Tofail, Kenitra, Morocco

⁴Energy, Materials and Sustainable Development Team, École Supérieure de Technologie - Salé, Mohammed V University, Rabat, Morocco

⁵Chemistry and Microbiology laboratories, Silviculture and Forest Health Service, National Agency for Water and Forests, Rabat, Morocco

*E-mail: oumaima_ninich@um5.ac.ma

Abstract

Cedar tar was obtained from a local producer located in Timhdite, Morocco, and it was subsequently cleaned using distilled water. The chemical composition analysis of both the uncleaned (UNC-CDT) and cleaned (C-CDT) cedar tar was performed using gas chromatography (GC-MS). To investigate its inhibitory effect on E24 steel corrosion in a 1 M HCl solution, electrochemical impedance spectroscopy and Tafel polarization curves were employed. The study also examined the influence of concentration and temperature on the inhibition's effectiveness, and the surface morphology was analyzed through SEM-EDX. The chemical composition analysis revealed that both UNC-CDT and C-CDT were characterized by three main compounds with the highest percentages: epi- β -Caryophyllene at 15.78% and 13.27%, followed by α -himachalene at 7.89% and 8.13%, and finally, (E)-Atlantone present at 6.06% and 5.21%, respectively. The electrochemical measurements showed that the inhibitory effect of Cedar Tar increased with concentration, reaching 93.09% and 95.51% at 1.5 g/L for UNC-CDT and C-CDT, respectively, at 293 K. The study observed that the organic components of cedar tar bind to metal surfaces through chemical and physical adsorption. The inhibitor exhibited good adsorption on the surface of E24 steel, following the Langmuir adsorption isotherm. As the inhibitor concentration increased, a thicker layer of inhibitor effectively covered the surface. In a 1 M hydrochloric acid solution, cedar tar proved to be an efficient corrosion inhibitor for E24 steel. Further studies are required to deepen our understanding and assess the full potential of wood tar as a corrosion inhibitor.

Keywords: cedar tar, corrosion inhibition, E24 steel, 1 M HCl, electrochemical techniques, SEM-EDX.

1. Introduction

Corrosion phenomena in steel have been a significant issue in numerous industrial applications worldwide, drawing the attention of researchers seeking effective solutions [1, 2]. During application, steel exhibits weak resistance to corrosion due to its inability to passivate in corrosive environments [3]. Consequently, extensive damage occurs, leading to high maintenance, repair, and corrosion costs [4]. Addressing corrosion control is crucial from an application standpoint, and the utilization of inhibitors plays a pivotal role in mitigating corrosion attacks and reducing environmental aggressiveness [5]. An emerging trend in finding effective corrosion inhibitors for metals in acidic mediums involves the use of environmentally safe and readily available natural products, such as plant extracts [6]. Essential oils, among these natural products, have gained popularity as eco-friendly corrosion inhibitors, proving their effectiveness in various studies [5–8]. The corrosion-inhibiting properties of essential oils are attributed to their phytochemical constituents [6], which adsorb onto the surface of the metal, effectively blocking active sites and consequently reducing the corrosion rate [6]. Apart from essential oils, wood tar is another type of plant extract produced through the pyrolysis of different vegetable matter from various species [9–11]. Although wood tar has been the subject of research in various domains, only two research papers have investigated its use as a green inhibitor. These studies evaluated the essential oil of cedar tar [8] and *Olea europaea* Subsp. *Cuspidata* wood tar [12] as potential corrosion inhibitors.

In this research paper, our main objective was to test and compare the corrosion protection ability of two types of cedar tar: uncleaned cedar tar (UNC-CDT) and cleaned cedar tar (C-CDT), as green inhibitors for E24 steel in a 1 M HCl solution. To assess the performance of both samples, we conducted electrochemical tests using potentiodynamic polarization (PP) and electrochemical impedance spectroscopy (EIS). Additionally, we examined the surfaces of the steel samples using scanning electron microscopy with energy-dispersive X-ray analysis (SEM-EDX).

2. Experimental

2.1. Inhibitor

The cedar tar, used as a green inhibitor in this study, was obtained from a local producer in Morocco, situated in Timhdite, Azrou region, in February 2022. A portion of the cedar tar sample (UNC-CDT) was subjected to multiple rounds of purification using distilled water until the water became clear [13, 14]. The purified cedar tar, referred to as C-CDT tar, was then stored in a bottle at 4°C [14] (Figure 1).

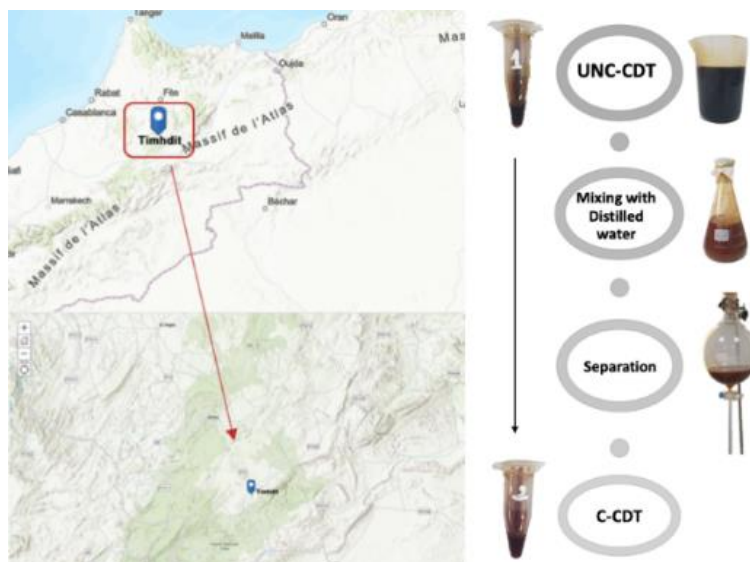


Figure 1. Geographical location of Timhdite and cedar tar samples preparation.

2.2. Material and solution

The carbon steel (E24) samples that was utilized in this study exhibited the following chemical composition (in wt%): Mn = 0.52%, Si = 0.20%, C = 0.16%, S = 0.009%, P = 0.007% and the remaining balance was Fe. Circular coupons of carbon steel were prepared, each having a diameter of 1 cm. Before conducting any measurements, the surface of the coupons that was exposed underwent mechanical abrasion using abrasive paper with specific grades 1000, 1500 and 2000. Subsequently, the specimens were rinsed with distilled water, degreased using ethanol, and subsequently dried using airflow. As for the corrosive solution, a 1 M HCl solution was prepared by diluting 37% HCl with distilled water. Prior to the electrochemical tests, pre-trials were conducted to determine the appropriate concentration ranges of cedar tar. Ultimately, the selected concentration ranges for the electrochemical tests were 0.5 g/L to 1.5 g/L.

2.3. Chromatographic GC-MS analysis

The analysis of both UNC-CDT and C-CDT was conducted using gas chromatography (GC) coupled to mass spectrometry (MS) at the Moroccan Foundation for Advanced Science, Innovation, and Research (MASeIR) Institute, following the conditions described in Skanderi's research paper. Cedar tar samples were diluted in chloroform and analyzed under the following conditions "an HP-5MS capillary column (5% phenyl 95% dimethylpolysiloxane, 30 m×0.25 mm i.d., 0.25 µm film thickness); Helium (purity: N 6.0) as the carrier gas; a flow rate of 0.5 mL/min; injection mode set to splitless; a solvent delay of 3 min; an injection volume of 0.2 µL; an injection temperature of 300°C; and an oven temperature programmed from 50°C to 250°C at a heating rate of 5°C/minute with a 15-minute hold at 250°C. The ionization mode used was electronic impact at 70 eV." The compounds' identification was carried out using the NIST 2017 MS Library [15].

2.4. Electrochemical measurements

The potentiodynamic polarization measurements were carried out in a standard three-electrode electrolytic cell. The selected reference electrode was a saturated calomel electrode (SCE), while the auxiliary electrode was made of platinum. As for the working electrode (E24 steel), a small circular piece with a 1 cm diameter was utilized. To control the measurements, we utilized the Voltalab (PGZ 100) connected to a personal computer running Volta Master 4 software for our experiments [16]. The sweep rate used was 10 mV/s, starting from an initial potential of -800 mV and ending at -100 mV relative to SCE. Before recording each curve, we allowed a stabilization period of 60 min to ensure a stable value for the free corrosion potential E_{corr} . The corrosion current densities were subsequently derived from the polarization curves by linearly extrapolating the Tafel curves. Furthermore, the same equipment was used for electrochemical impedance spectroscopy (EIS). After determining the steady-state current at a particular potential, a wave voltage with a peak-to-peak amplitude of 10 mV was superimposed on the resting potential. The measurements at the resting potential were automated through computer programs after 60 min of exposure. We represented impedance diagrams using the Nyquist plot [17, 18].

2.5. Surface morphology

Scanning Electron Microscopy (SEM) equipped with Energy Dispersive X-ray (EDX) was employed to analyze the surface structure and elemental composition of carbon steel samples after 24 h of exposure to a corrosive solution, with and without uncleaned and cleaned cedar tar. The analysis was carried out at the Laboratoire MEB-EDX, one of the Technical Support Units for Scientific Research under the National Center for Scientific and Technical Research.

3. Results and Discussion

3.1. Chromatographic GC-MS analysis

We have marked with green circles distinctive peaks on the chromatogram of both uncleaned and cleaned cedar tar. The results are depicted in Figure 1, indicating characteristic compositions of the UNC-CDT and C-CDT samples (Table 1). Among the highlighted components, one molecule stands out with the highest percentage in both samples, appearing at a retention time (RT) of 17.275. This molecule is identified as (1*R*,9*R*,*E*)-4,11,11-trimethyl-8-methylenebicyclo[7.2.0]undec-4-ene, commonly known as epi- β -caryophyllene, with percentages of 15.78% and 13.27%, respectively. Following that, the second-highest percentage belongs to 1*H*-Benzocycloheptene, 2,4*a*,5,6,7,8,9,9*a*-octahydro-3,5,5-trimethyl-9-methylene-, (4*aS*-*cis*-), also referred to as α -himachalene, with percentages of 7.89% and 8.13%, respectively. In the third position, we identified (*E*)-atlantone, which was present at 6.06% and 5.21%, respectively. The fourth place includes 5-hydroxy-6-methoxy-8-[(4-amino-1-methylbutyl)amino]quinoline trihydrobromide, known as γ -himalachene, with

percentages of 4.27% and 5.88%. Lastly, in the fifth position among the most characteristic compounds, we found 4-acetyl-1-methylcyclohexene, with percentages of 2.52% and 1.6% for the uncleaned and cleaned tar, respectively.

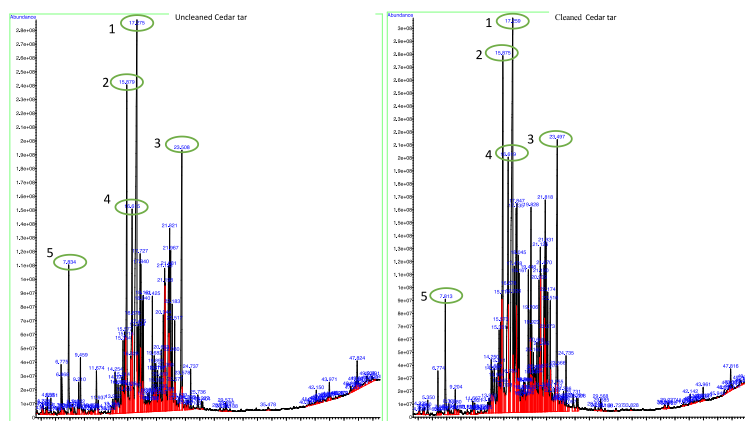


Figure 1. Chromatogram of the composition of uncleaned and cleaned Cedar Tar.

Table 1. Percentage (%) of constituent compounds in uncleaned and cleaned Cedar Tar.

Compound	RT	UNC-CDT	C-CDT
2-Methyl-2-cyclopenten-1-one	3.433	0.02	—
1-Ethyl-3-methyl-benzene	4.098	—	0.06
1-Ethyl-2-methyl-benzene	4.143	0.29	0.10
5-Methyl-2-furancarboxaldehyde	4.290	0.12	—
3-Methyl-3-cyclohexen-1-one	4.662	0.10	0.06
2,4,6-Trimethyl-benzoic acid, 5-methylene-1,3a,4,5,6,6a-hexahydropentalen-1-ylester	4.763	0.05	0.04
1-Ethenyl-2-methyl-benzene	4.864	0.21	—
1-Ethenyl-3-methyl-benzene	4.864	—	0.06
O-Cymene	5.349	0.27	1.02
2,3-Dimethyl-2-cyclopenten-1-one	5.710	0.03	—
Indene	5.777	0.03	—
2-Methyl-phenol	6.341	0.09	—
3-Ethenyl-1,2-dimethyl-1,4-cyclohexadiene	6.656	0.04	—
O-Isopropenyltoluene	6.667	—	0.03
1-Methyl-4-(1-methylethenyl)-benzene	6.780	0.39	0.31
2-Methoxy-phenol	6.870	0.69	—
3-Methyl-phenol	6.983	—	0.05

Compound	RT	UNC-CDT	C-CDT
<i>p</i> -Cresol	7.084	0.10	–
4-Methyl-1,3-heptadiene	7.084	–	0.06
2-Methyl-benzofuran	7.220	0.09	0.04
4-Acetyl-1-methylcyclohexene	7.839	2.52	1.6
1-Methyl-1 <i>H</i> -indene	8.200	0.08	0.07
Decamethyl-cyclopentasiloxane	8.313	0.14	0.16
3-Cyclohexene-1-methanol, .alpha.4-dimethyl-	8.380	0.08	–
2,3-Dimethyl-phenol	8.628	0.17	–
2,4-Dimethyl-phenol	8.639	–	0.11
Naphthalene	9.079	0.17	0.15
1-(4-Methylphenyl)-ethanone	9.214	0.51	0.35
Creosol	9.459	1.00	0.10
1,5,5-Trimethyl-6-methylene-cyclohexene	9.676	–	0.05
5,6-Dimethyl-1 <i>H</i> -benzimidazole	9.879	0.14	–
2-Ethenyl-1,3,5-trimethyl-benzene	10.093	0.09	–
1,3-Dimethyl-1 <i>h</i> -indene	11.040	0.20	0.07
1 <i>H</i> -1,5-Benzodiazepine, 2,3,4,5-tetrahydro-2,4-dimethyl-	11.389	–	0.06
4-Ethyl-2-methoxy-phenol	11.671	0.98	0.30
2-Methyl-naphthalene	11.941	0.22	0.23
Dodecamethyl-cyclohexasiloxane	12.786	–	0.09
4- <i>tert</i> -Butyltoluene	12.899	–	0.03
1,2,3,4-Tetrahydro-1,1,6-trimethyl-naphthalene	13.327	2.47	0.06
2,5-Dimethoxyethylbenzene	13.767	0.21	–
8,8,9,9-Tetramethyl-3,4,5,6,7,8-hexahydro-2 <i>H</i> -2,4a-methanonaphthalene	13.857	0.06	0.33
2-Methoxy-4-propyl-phenol	13.947	0.29	0.25
(1,1,2-Trimethylpropyl)-benzene	14.251	0.79	–
5,6,7,8-Tetrahydroindolizine	14.386	–	0.75
10,10-Dimethyl-2,6-dimethylenebicyclo[7.2.0]undecane	14.398	0.67	–
Gamma-muurolene	14.668	0.93	1.18
2,3-Dihydro-1,1,3-trimethyl-1 <i>h</i> -indene	14.972	0.57	–

Compound	RT	UNC-CDT	C-CDT
2,6-Dimethyl-naphthalene	15.209	0.70	–
Alpha-farnesene	15.356	2.48	–
1,2,3,4-Tetrahydro-1,5-dimethyl-naphthalene	15.457	0.23	0.52
1,6-Dimethyl-naphthalene	15.209	–	0.86
1,2,3,4-Tetrahydro-8-methyl-1-naphthalenemethanol	15.468	–	0.29
1 <i>H</i> -Benzocycloheptene,2,4a,5,6,7,8,9,9a-octahydro-3,5,5-trimethyl-9-methylene-, (4 <i>as-cis</i>)-	15.716	7.89	8.13
Trans-isoeugenol	16.099	0.56	–
5-Hydroxy-6-methoxy-8-[(4-amino-1-methylbutyl)amino]quinolinetrihydrobromide	16.426	1.03	–
Tricyclo[5.4.0.0(2,8)]undec-9-ene,2,6,6,9-tetramethyl-,(1 <i>R</i> ,2 <i>S</i> ,7 <i>R</i> ,8 <i>R</i>)-	16.099	–	0.41
5-Hydroxy-6-methoxy-8-[(4-amino-1-methylbutyl)amino]quinoline trihydrobromide	16.618	4.27	5.88
Di-epi-.alpha.-cedrene-(<i>i</i>)	16.674	0.99	0.95
1-(1,5-Dimethyl-4-hexenyl)-4-methyl-benzene	16.787	0.59	0.75
(1 <i>R</i> ,9 <i>R</i> , <i>E</i>)-4,11,11-Trimethyl-8-methylenebicyclo[7.2.0]undec-4-ene	17.271	15.78	13.27
Benzene,1-methyl-4-(1,2,2-trimethylcyclopentyl)-, (<i>R</i>)-	17.339	1.53	1.81
Alpha.-dehydro-ar-himachalene	17.474	1.14	1.52
Naphthalene,1,2,3,5,6,8a-hexahydro-4,7-dimethyl-1-(1-methylethyl)-, (1 <i>s-cis</i>)-	17.722	3.31	3.81
Gamma-dehydro-ar-himachalene	17.835	2.23	2.68
Ar-himachalene	18.038	1.37	–
1-Methyl-7,11-dithiaspiro[5,5]undecane	18.049	–	1.68
4-Isopropyl-6-methyl-1-methylene-1,2,3,4-tetrahydronaphthalene	18.161	2.05	2.25
Gamma-himachalene	18.511	–	0.18
6-Methyl-2-(4-methylcyclohex-3-en-1-yl)hepta-1,5-dien-4-ol	18.702	–	0.15
(4 <i>aS</i>)-3,5,5,9-Tetramethyl-1,2,5,6,7,8-hexahydro-4 <i>a</i> ,8-epoxybenzo[7]annulene	18.916	–	0.31
1 <i>H</i> -Indene,1-ethenyl-2,3-dihydro-	19.131	0.15	0.19
(+/-)-Dihydro-ar-turmerone	19.424	1.80	1.90
4-(2,4-dimethylcyclohex-3-enyl)but-3-en-2-one	19.581	0.30	–
Propane,2-cyclohexyl-2-phenyl-	19.683	0.77	–
Cis-.alpha.-copaene-8-ol	19.705	–	1.61

Compound	RT	UNC-CDT	C-CDT
(+)-.Beta.-himachaleneoxide	19.784	0.54	–
Beta-himachalenoxide	19.897	0.65	2.62
1(2 <i>H</i>)-Naphthalenone,octahydro-4,8a-dimethyl-6-(1-methylethenyl)-, (4.alpha.,4a.beta.,6.alpha.,8a.beta.)-	19.919	–	0.83
(1 <i>R</i> ,4 <i>R</i> ,5 <i>S</i>)-1,8-dimethyl-4-(prop-1-en-2-yl)spiro[4.5]dec-7-ene	19.976	0.40	0.47
Epicubenol	20.156	0.77	0.96
1,1'-Biphenyl,4-(1-methylethyl)-	20.291	0.20	0.49
(3 <i>S</i> ,3 <i>A</i> <i>S</i> ,6 <i>R</i> ,8 <i>A</i> <i>S</i>)-3,8,8-Trimethyl-7-methyleneoctahydro-1 <i>h</i> -3 <i>a</i> ,6-methanoazulene	20.381	–	0.47
2,4-Dimethoxy-benzonitrile	20.472	0.52	0.53
1 <i>H</i> -3 <i>a</i> ,7-Methanoazulene, 2,3,4,7,8,8a-hexahydro-3,6,8,8-tetramethyl-, [3 <i>r</i> -(3.alpha.,3a.beta.,7.beta.,8a.alpha.)]-	20.663	1.32	1.76
(3 <i>R</i> ,4 <i>a</i> <i>S</i> ,8 <i>a</i> <i>S</i>)-8a-Methyl-5-methylene-3-(prop-1-en-2-yl)- 1,2,3,4,4a,5,6,8a-octahydronaphthalene	20.776	–	0.45
(<i>Z</i>)-1-Methyl-4-(6-methylhept-5-en-2-ylidene)cyclohex-1-ene	20.945	2.07	4.48
Ar-Turmerone	21.136	2.90	2.32
1,3-Dimethyl-5-trifluoroacetoxycyclohexane	21.193	1.06	–
2,5-Dimethyl- <i>para</i> -anisaldehyde	21.193	–	1.33
Naphthalene, 1,6-dimethyl-4-(1-methylethyl)-	21.283	1.50	1.67
1,5-Dimethyl-7,11-dithiaspiro[5.5]undecane	21.384	0.38	–
4-(1 <i>H</i> -Imidazol-1-yl)-benzenamine	21.384	–	0.42
Tumerone	21.677	3.36	2.89
2,2,6-Trimethyl-6-(4-methylcyclohex-3-en-1-yl)dihydro-2 <i>H</i> -pyran- 4(3 <i>h</i>)-one	21.824	3.33	3.13
1,3-Diisopropenyl-6-methyl- cyclohexene	21.925	–	2.61
(<i>Z</i>)-.gamma.-atlantone	21.970	2.99	–
3,3,4-Trimethyl-4-(4-methylphenyl)-cyclopentanone	22.083	0.69	0.85
(<i>Z</i>)-alpha-atlantone	22.184	1.42	1.34
8-Quinolinemethanol	22.511	–	1.32
1,2,3,4-Tetrahydro-1,6-dimethyl-4-(1-methylethyl)-,(1 <i>S</i> - <i>cis</i>)- naphthalene	22.579	0.39	0.56
3-Methyl-2-butenic acid, 2,7-dimethyloct-7-en-5-yn-4-yl ester	22.804	0.23	0.38

Compound	RT	UNC-CDT	C-CDT
6-Isopropenyl-4,8a-dimethyl-1,2,3,5,6,7,8,8a-octahydro-naphthalen-2-ol	23.131	–	0.50
1-Chloro-5-methyl-hexane	23.142	0.30	–
(E)-Atlantone	23.503	6.06	5.21
2-(3-Ethyl-1 <i>H</i> -1,2,4-triazol-5-yl)phenol	23.582	0.33	0.40
2-Bromomethyl-2,3-dihydrobenzofuran	23.931	0.07	–
2,3-Pentadienoic acid, 2-methyl-4-phenyl-, ethyl ester	24.021	0.12	–
2,2,7,7-Tetramethyltricyclo[6.2.1.0(1,6)]undec-4-en-3-one	24.021	–	0.23
1 <i>H</i> -Indole-2-carboxylic acid, 1-methyl-	24.156	–	0.14
2-Methyl-6-methyleneocta-2,7-dien-4-one	24.247	–	0.23
Neoisolongifolene, 8-bromo-	24.393	0.19	0.41
Boron, difluoro[1-(2-hydroxy-4-methoxyphenyl)ethanonato]-, (t-4)-	24.742	0.51	0.75
(2-Hydroxy-4,5-dimethylbenzoyl)formic acid	25.103	0.05	0.15
Naphthalene, 6-(1-ethylpropyl)-1,2,3,4-tetrahydro-	25.734	0.29	–
1 <i>H</i> -Pyrazole-3-propanol, 5-(4-methylphenyl)-	26.230	0.12	–
Dodecanoic acid, <i>n</i> -octyl ester	25.734	–	0.38
Cinnoline, 4-ethyl-3-methyl-	26.219	–	0.23
Hexadecanoic acid, methyl ester	26.410	0.10	0.18
7-Isopropyl-1,1,4 <i>a</i> -trimethyl-1,2,3,4,4 <i>a</i> ,9,10,10 <i>a</i> -octahydrophenanthrene	28.822	0.05	0.05
(4 <i>aS</i> ,4 <i>bR</i> ,10 <i>aS</i>)-7-Isopropyl-1,1,4 <i>a</i> -trimethyl-1,2,3,4,4 <i>a</i> ,4 <i>b</i> ,5,6,10,10 <i>a</i> -decahydrophenanthrene	29.261	0.04	0.03
9,12-Octadecadienoic acid(<i>Z,Z</i>)-, methyl ester	29.577	0.11	0.11
9-Octadecenoic acid(<i>Z</i>)-, methyl ester	29.689	0.08	0.08
Methyl stearate	30.185	0.04	0.04
Benzene, 1,1'-selenobis-	31.740	–	0.04
Methyl dehydroabietate	33.825	–	0.03
1 <i>H</i> -Inden-5-ol, 2,3-dihydro-3-(4-hydroxyphenyl)-1,1,3-trimethyl-	35.481	0.10	–
Allopregnane-3.α.,20.α.-diol	38.546	–	0.09
Pyrene, 2-methyl-	38.637	–	0.04
2-Aminocaprylic acid, <i>n</i> -(2-methoxyethylcarbonyl)-, dodecyl ester	39.031	–	0.1
Fluoranthene, 2-methyl-	39.121	–	0.02

Compound	RT	UNC-CDT	C-CDT
11,12-Dihydroxyseychellane	40.890	0.03	–
4-Bromo- <i>n</i> -[2-[1-(4-bromophenyl)-5-tetrazolyl]ethenyl]-benzenamine	41.093	–	0.01
7 <i>H</i> -Dibenzo[<i>de,g</i>]quinolin-7-one, 1,2,9,10-tetramethoxy-	41.206	–	0.04
2,4-Diamino-6-[[4-phenyl-2-thiazolyl]thio]quinazoline	41.217	0.07	–
2-(Triethoxysilyl)-ethanethiol	41.544	–	0.02
3-(Triethoxysilyl)propanenitrile	41.555	0.04	–
Thiazolo[3,2- <i>a</i>]benzimidazol-3(2 <i>H</i>)-one, 6,8-dimethyl-2-(3-nitrobenzylideno)-	42.152	0.25	–
4-(2',4',4'-Trimethylcyclo[4.1.0]hept-2'-en-3'-yl)-3-buten-2-one	42.310	0.04	0.03
1-Methoxy-2-(1-methyl-2-methylenecyclopentyl)-benzene	42.389	–	0.04
<i>N</i> -(2,3,5,6,7,8-tetrahydro-1 <i>H</i> -cyclopentano[<i>b</i>]quinolin-9-yl)-heptanamide	42.400	0.06	–
2-Methoxy-4-methyl-3-nitro-, methyl-benzoic acid	42.682	–	0.05
Ethyl 6-amino-4-[<i>p</i> -chloroanilino]-5-nitro-2-pyridinecarbamate	43.054	0.07	0.19
2-Pyridinamine, <i>n</i> -(4,5-dihydro-5-methyl-2-thiazolyl)-3-methyl-	43.786	0.11	0.06
<i>N</i> -Octyltriethoxysilane	43.967	0.35	–
2-(4-Ethoxyphenyl)-2-methyl-propanal	43.967	–	0.19
2-(4-Methylbenzoyl)-, benzoic acid methyl ester	44.147	0.13	0.02
1,2-Benzisothiazole-3-acetic acid, methyl ester	45.285	0.03	–
<i>N</i> -(3-Chlorophenyl)maleimide	45.477	0.02	–
Silane, diphenyl(<i>cis</i> -hex-3-en-1-yloxy)dodecyloxy-	46.942	0.18	–
4-Methyl- <i>n</i> -(triphenylphosphoranylidene)-benzenamine	47.223	–	0.09
2-(<i>N</i> -Propyl)oxybenzylideneacetophenone	47.449	0.07	–
2-[2-[2-(4-Chloro-phenoxy)-ethylsulfanyl]-benzoimidazol-1-yl]-acetamide	47.651	0.23	0.18
28-Norolean-17-en-3-one	47.821	0.60	0.35
1 <i>H</i> -Pyrazole-1-acetamide, 4-iodo- <i>n</i> -(4-pyridinylmethyl)-	48.925	0.20	0.01
4-Chloro-6-methoxy-2-methylquinolin-8-amine	49.240	0.04	0.07
Hexamethyl-cyclotrisiloxane	49.229	–	0.23
2,4-Dimethyl-benzo[<i>h</i>]quinoline	49.894	0.20	0.18
Thymol, tbdms derivative	50.288	0.02	–

According to previous studies, Atlas cedar tar (*Cedrus atlantica*) is primarily composed of hydrocarbon sesquiterpenes, including cadinene stereoisomers, α -cedrene, 5-*epi*-aristolochene, and benzocycloheptene. It also contains oxygenated sesquiterpenes such as (α , β , and γ) Himachelene, Tumerone, Ar-tumerone, α -Atlantone, and Himachalol [9–14, 19–22]. In Skanderi's study on the chemical characterization of cedar tar in Algeria, researchers identified 88 components representing 76% of the tar, with β -himachalene being the most abundant at 14.51%. Comparing our results, we did not find *epi*- β -caryophyllene, which, in our case, was the dominant compound. Instead, we observed all other compounds with lower percentages compared to their results, specifically 4.53%, 5.15%, 4.07%, and 0.48% for α -himachalene, (*E*)-atlantone, γ -himalachene, and 4-acetyl-1-methylcyclohexene, respectively [15]. In another study focusing on Lebanese cedar tar, 41 compounds were identified, with β -himachalene being the main compound at 22–28%. α -Himachalene was present in smaller amounts (6–10%), along with *E*-(α)-atlantone [23].

Our findings are consistent with previous studies, indicating the presence of several important compounds in Atlas cedar tar, such as β -himachalene, α -himachalene, and atlantone, among others. In Morocco, essential oil extracted from *Cedrus atlantica* sawdust was analyzed by GC and GC/MS, identifying 53 components, with the three isomers of himachalene being predominant and smaller amounts of (*E*) and (*Z*) isomers of atlantone were also present [24]. The chemical composition of *Cedrus* species, especially essential oils, has been widely studied. However, to the best of our knowledge, only a few studies have investigated the composition of wood tar obtained from *Cedrus atlantica*. According to Burri *et al.*, Atlas cedar tar remains largely unexplored and has not been thoroughly studied analytically. Although some tars produced in Morocco through technical charcoal-burning processes have been analyzed [9].

3.2. Potentiodynamic polarization

3.2.1. Concentration effect

The results represented in Figure 2 show the potentiodynamic polarization curves for E24 steel immersed in a 1 M HCl solution, both in the absence and presence of Cedar Tar at a temperature of 293 K. These curves provide valuable insights into the electrochemical parameters, which include the corrosion potential (E_{corr}), corrosion current density (i_{corr}), anodic (β_a) and cathodic (β_c) Tafel constants. These parameters that are crucial for assessing the corrosion behavior were derived from the Tafel plots.

An interesting observation emerges from the potentiodynamic polarization curves, revealing a notable reduction in both anodic and cathodic current densities in the presence of Cedar Tar. This outcome can be attributed to the adsorption of organic compounds present in both the uncleaned Cedar Tar (UNC-CDT) and cleaned Cedar Tar (C-CDT) onto the active sites of the electrode surface. This adsorption phenomenon effectively retards the dissolution of metallic components and the evolution of hydrogen, indicative of a mixed-type behavior exhibited by Cedar Tar. Consequently, this interaction serves to decelerate the

overall corrosion process [8–25]. These findings align with the research outcomes of Turkustani *et al.* and Jaouadi *et al.* [8–12].

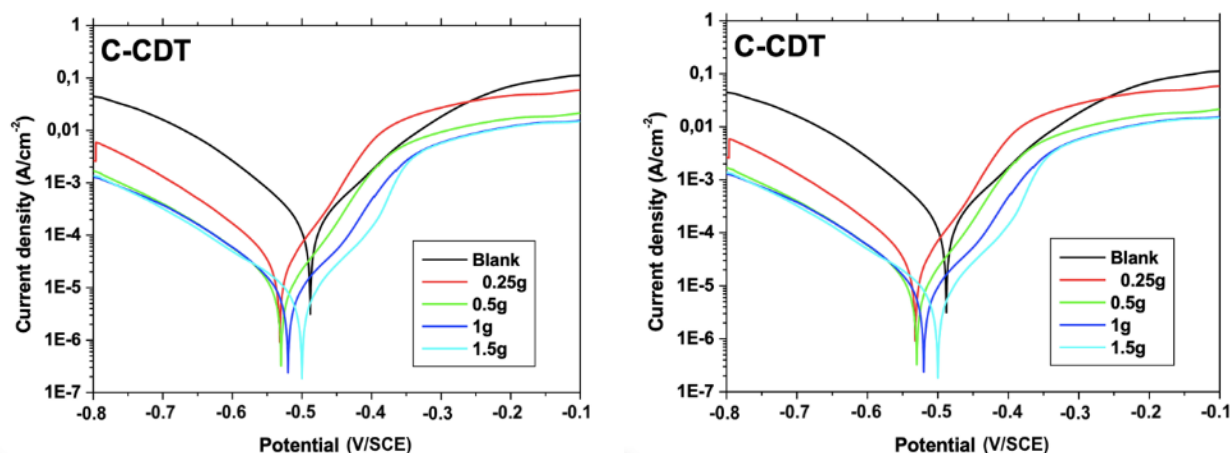


Figure 2. Cathodic and anodic polarization curves of E24 steel in 1 M HCl at different concentrations of UNC-CDT and C-CDT.

The electrochemical parameters, such as corrosion potential (E_{corr}), corrosion current density (i_{corr}), and the anodic and cathodic Tafel slopes (β_c and β_a), for varying concentrations of Cedar Tar (UNC-CDT and C-CDT), are presented in Table 2. The β_c and β_a values are computed from the linear segments of the polarization curves, while i_{corr} is determined at the point where the linear portion of the cathodic curves intersects with the corresponding stationary corrosion potential.

The inhibition efficiency ($IE\%$) is assessed based on the i_{corr} values, utilizing Equation 1.

$$IE\% = \frac{i_{\text{corr}}^0 - i_{\text{corr}}^{\text{inh}}}{i_{\text{corr}}^0} \cdot 100 \quad (1)$$

The corrosion current densities in the absence and presence of UNC-CDT and C-CDT inhibitors, denoted as i_{corr}^0 and $i_{\text{corr}}^{\text{inh}}$, respectively, are determined through the extrapolation of the anodic and cathodic Tafel lines to E_{corr} .

Table 2. Corrosion inhibition parameters and their corresponding inhibition efficiencies for E24 in 1 M HCl solution in the absence and presence of various concentrations of UNC-CDT and C-CDT.

Inhibitor	C_{inh} , g/L	E_{corr} , mV/SCE	i_{corr} , $\mu\text{A}/\text{cm}^2$	β_c , mV/dec	β_a , mV/dec	$IE\%$
None	0.0	−488	174.8	−94.7	93.3	—
UNC-CDT	0.25	−505	35.94	−103.0	49.5	79.44
	0.5	−491	20.49	−130.2	44.2	88.28
	1.0	−483	17.71	−121.5	56.8	89.87
	1.5	−473	12.08	−128.6	41.6	93.09

Inhibitor	C_{inh} , g/L	E_{corr} , mV/SCE	i_{corr} , $\mu\text{A}/\text{cm}^2$	β_c , mV/dec	β_a , mV/dec	$IE\%$
C-CDT	0.25	−532	16.41	−102.9	55.8	90.61
	0.5	−530	13.97	−111.2	61.0	92.01
	1.0	−520	10.01	−103.8	80.6	94.28
	1.5	−500	7.85	−111.3	77.7	95.51

It can be observed from Table 2 that the addition of the inhibitor to the studied medium significantly reduced the corrosion current density (i_{corr}), bringing it down to only $12.08 \mu\text{A}/\text{cm}^2$ and $7.85 \mu\text{A}/\text{cm}^2$ for UNC-CDT and C-CDT, respectively. Furthermore, the inhibition efficiency calculated from the i_{corr} values obtained in the presence of cedar tar samples ranged from 79.44% to 93.09% for UNC-CDT and from 90.61% to 95.51% for C-CDT over a concentration range of 0.25–1.5 g/L. These results demonstrate that both Cedar Tar samples can efficiently protect E24 steel from dissolution in 1 M HCl solution, particularly C-CDT at a concentration of 1.5 g/L.

3.2.2. Effect of Temperature

To assess the impact of temperature on the corrosion of E24 steel, we performed potentiodynamic polarization measurements across a temperature spectrum ranging from 293 K to 323 K, both in the absence and presence of UNC-CDT and C-CDT. The resulting polarization curves are represented in Figure 3, and the electrochemical parameters are detailed in Figure 3. Potentiodynamic polarization curves for the corrosion of E24 steel at different temperatures, with and without cedar tar samples (1.5 g/L) in a 1 M HCl solution.

Table 3.

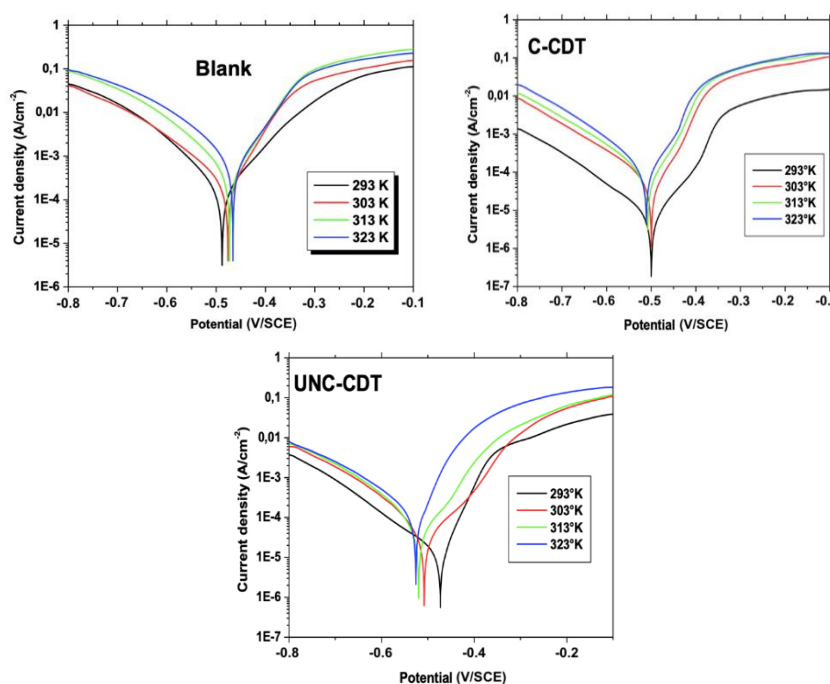


Figure 3. Potentiodynamic polarization curves for the corrosion of E24 steel at different temperatures, with and without cedar tar samples (1.5 g/L) in a 1 M HCl solution.

Table 3. Corrosion parameters obtained from potentiodynamic polarization of E24 steel in 1 M HCl, with and without the addition of 1.5 g/L of UNC-CDT and C-CDT, at various temperatures.

Inhibitor	Temperature, K	E_{corr} , mV/SCE	i_{corr} , $\mu\text{A}/\text{cm}^2$	IE%
Blank	293	−488	174.8	—
	303	−476	234.7	—
	313	−473	341.7	—
	323	−466	735.6	—
UNC-CDT	293	−473	12.08	93.09
	303	−508	36.25	84.56
	313	−520	52.6	84.60
	323	−526	91.4	87.57
C-CDT	293	−500	7.85	95.51
	303	−500	62.54	74.48
	313	−508	86.21	74.34
	323	−511	120.77	82.84

Based on the results presented in Figure 3. Potentiodynamic polarization curves for the corrosion of E24 steel at different temperatures, with and without cedar tar samples (1.5 g/L) in a 1 M HCl solution.

Table 3, we can observe that as the temperature rises, there is a corresponding increase in the corrosion current density (i_{corr}), and a slight decrease in the inhibition efficiency values. This observed phenomenon can be attributed to the desorption of certain inhibitor molecules from the surface of the E24 steel, driven by the temperature elevation.

It's important to emphasize that in the absence of Cedar Tar samples, the current density values experience a significant spike at higher temperatures when compared to the inhibited solution. However, when Cedar Tar samples are introduced, the dissolution of E24 steel is markedly inhibited. This intriguing effect can be attributed to a decrease in the adsorption process with the increase in temperature, suggesting a physical adsorption mechanism at play [26, 27].

At 323 K, in the absence of any inhibitor, there is a significant increase in the corrosion current density (i_{corr}) with a value of 735.6 $\mu\text{A}/\text{cm}^2$ compared to lower temperatures. When inhibitors are introduced, there is a notable improvement in inhibition efficiency as the temperature increases. For the UNC-CDT inhibitor, i_{corr} is reduced to 91.4 $\mu\text{A}/\text{cm}^2$, while the C-CDT inhibitor results in i_{corr} decreasing to 120.77 $\mu\text{A}/\text{cm}^2$. These results imply that the

corrosion rate significantly rises without an inhibitor as the temperature increases, likely due to the accelerated corrosion reactions at higher temperatures. Conversely, in the presence of an inhibitor, there is a reduction in the rate of corrosion, indicating that both inhibitors are effective at elevated temperatures. The data further suggests that UNC-CDT is particularly proficient at inhibiting corrosion at higher temperatures, resulting in a lower corrosion rate. The observed enhancement in inhibition efficiency at 323 K for both UNC-CDT and C-CDT can be attributed to a multifaceted interplay of factors. Firstly, there is a likely augmentation in adsorption onto the metal surface at elevated temperatures, thereby improving the corrosion inhibitors' effectiveness. Secondly, the kinetics of corrosion reactions, being temperature-dependent, may contribute to heightened inhibitor efficacy. Additionally, variations in solution properties, such as pH and the presence of ions, could influence inhibitor interactions with corrosive species differently at higher temperatures, offering increased protection. Furthermore, thermodynamic considerations suggest that the equilibrium of corrosion reactions may shift at elevated temperatures, amplifying the inhibitors' impact on the overall corrosion rate. It's crucial to acknowledge that the precise inhibition mechanism is intricate and contingent on the specific inhibitor and corrosive environment, necessitating further experimental data and a nuanced understanding of the inhibitor's behavior under diverse conditions for a more accurate explanation [5, 28–30].

Figure 4 illustrates the corrosion reaction as an Arrhenius-type process. We estimated the activation parameters (E_a , ΔH_a and ΔS_a) using the Arrhenius Equation 2 and the transition state Equation 3. These values are detailed in Table 4.

$$i_{\text{corr}} = A \exp\left(-\frac{E_a}{RT}\right) \quad (2)$$

$$i_{\text{corr}} = \frac{RT}{Nh} \exp\left(-\frac{\Delta S_a}{R}\right) \exp\left(-\frac{\Delta H_a}{RT}\right) \quad (3)$$

In the equation, (A) represents the pre-exponential factor, E_a stands for the apparent energy of activation for corrosion, N denotes Avogadro's constant, and h is the Planck constant. Additionally, ΔH_a and ΔS_a indicate the enthalpy and entropy changes of activation energy for the corrosion transition state complex, with R representing the gas constant.

The apparent activation energy is determined from the slopes of $\ln(i_{\text{corr}})$ vs. $1/T$. Consequently, the values of ΔH_a and ΔS_a are then computed from the $\ln(i_{\text{corr}}/T)$ vs. $1/T$ graphs.

It is worth noting that the temperature dependency of the inhibition effect, along with the comparison of apparent activation energy (E_a) values for the corrosion process in the presence and absence of inhibitors, can offer valuable insights into the mechanism of the inhibition action [26–28].

However, it is widely acknowledged that understanding the temperature-dependent nature of the inhibition effect, along with comparing the apparent activation energy values,

E_a for the corrosion process in the absence and presence of inhibitors, can offer additional insights into the mechanism of inhibition [31–33].

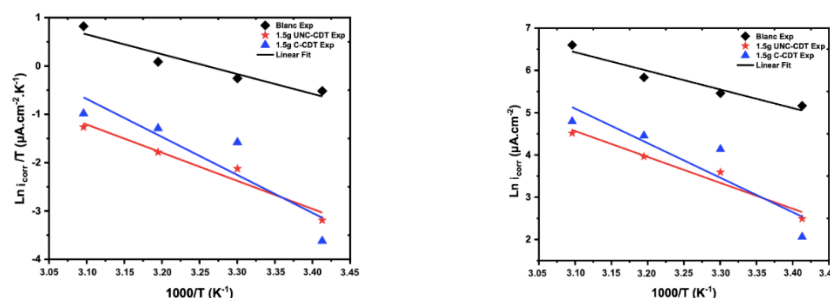


Figure 4. Variation of $\ln(i_{\text{corr}})$ and $\ln(i_{\text{corr}}/T)$ as a function of $1000/T$ in a 1 M HCl solution in the absence and in the presence of 1.5 g of UNC-CDT and C-CDT at different temperatures.

The data presented in Table 4 reveals positive values for both E_a (activation energy) and ΔH_a (enthalpy of activation), signifying the endothermic nature of the corrosion process. Specifically, the values for UNC-CDT are 50.95 kJ/mol for E_a and 48.39 kJ/mol for ΔH_a . While those for C-CDT are 67.90 kJ/mol for E_a and 65.34 kJ/mol for ΔH_a . These higher values of E_a and ΔH_a in the presence of the inhibitor, indicate an increased energy barrier for the corrosion reaction. This, in turn, leads to a more pronounced hindrance of the corrosion process, with surface sites exhibiting progressively higher E_a values [8].

The substantial elevation in the activation energy when the inhibitor is present can be attributed to its physical adsorption [34]. The inhibitor effectively obstructs certain active sites on the metal surface, resulting in a surface that is more energetically heterogeneous [35].

Conversely, the negative values of ΔS_a suggest that the activated complex in the rate-determining step represents an association rather than a dissociation step. This is indicative of a decrease in disorder as the reactants transition to the activated complex [36].

Table 4. Thermodynamic parameters of E24 steel in 1 M HCl solution without and with 1.5 g of UNC-CDT and C-CDT.

C_{inh} , g/L	E_a , kJ/mol	ΔH_a , kJ/mol	ΔS_a , kJ/mol·K
Blank	36.61	34.05	−86.52
UNC-CDT (1.5 g/L)	50.95	48.39	−57.58
C-CDT (1.5 g/L)	67.90	65.34	−0.63

3.3. Electrochemical impedance spectroscopy

EIS stands as an invaluable non-invasive method for assessing the corrosion inhibition characteristics within an electrochemical system [18].

Nyquist impedance plots were obtained for the E24 steel electrode at its respective corrosion potentials, after immersing it in 1 M HCl for 60 min at 293 K. These measurements were conducted both in the presence and absence of different concentrations of Cedar Tar samples. Figure 5 displays the resulting Nyquist plots, Bode plots, and phase angles. The figure illustrates that as the concentration of Cedar Tar samples increases, the diameter of the Nyquist plots also increases. Notably, the diameter of C-CDT is larger than that of UNC-CDT. The Nyquist plots exhibit one capacitive loop with one time constant, which can be attributed to the charge transfer process. However, these capacitive loops in this medium are not perfect semicircles. This phenomenon is probably a result of the frequency dispersion effect induced by the roughness and inhomogeneity nature of the electrode surface [37]. The inhibition efficiency ($E_{EIS} \%$) obtained from the charge transfer resistance can be estimated using the Equation 4:

$$E_{EIS} \% = \frac{R_{ct/inh} - R_{ct}}{R_{ct/inh}} \cdot 100 \quad (4)$$

where $R_{ct/inh}$ and R_{ct} represent the charge transfer resistances in inhibited and uninhibited solutions, respectively.

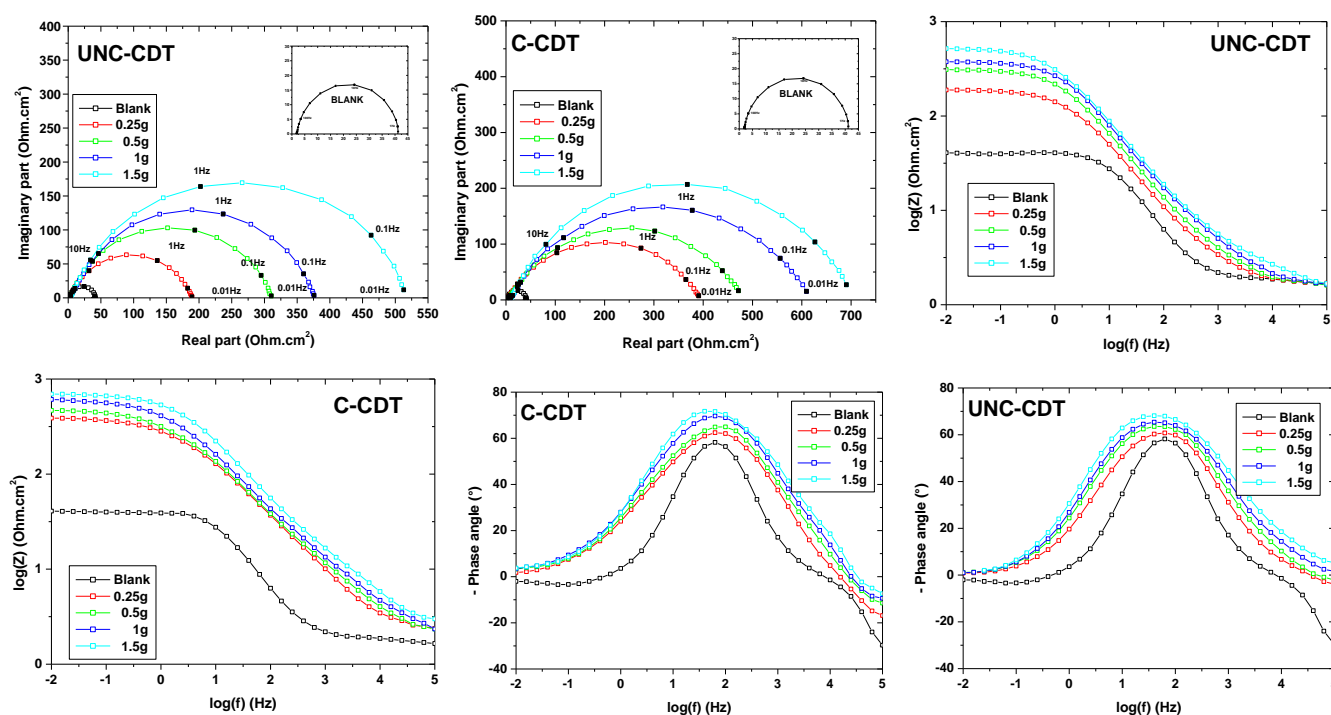


Figure 5. Nyquist, Bode and phase angle of E24 steel after 60 min of immersion in 1 M HCl solution without and with different concentrations of UNC-CDT and C-CDT at 293 K.

The polarization resistance values were determined through the subtraction of the high-frequency intersection from the low-frequency intersection [38]. We also calculated the

double-layer capacitance (C_{dl}) and identified the frequency at which the imaginary component of the impedance reaches its maximum (f_{max}) using Equation 5.

$$C_{dl} = \frac{1}{R_t 2\pi f_{max}} \quad (5)$$

where C_{dl} is the double layer capacitance ($\mu\text{F}/\text{cm}^2$); f_{max} is the maximum frequency (Hz); and R_t is the charge transfer resistance ($\Omega \cdot \text{cm}^2$).

Table 5. Electrochemical impedance parameters for the corrosion inhibition of the E24 steel in 1 M HCl solution without and with different concentrations of UNC-CDT and C-CDT.

Inhibitor	C_{inh} , g/L	R_s , $\Omega \cdot \text{cm}^2$	R_t , $\Omega \cdot \text{cm}^2$	C_{dl} , $\mu\text{F}/\text{cm}^2$	$IE\%$	θ
Blank	0	1.920	39.67	401.1	—	—
UNC-CDT	0.25	1.391	187.1	212.66	78.80	0.7880
	0.5	1.286	306.1	129.99	87.04	0.8704
	1	1.265	380.3	104.62	89.57	0.8957
	1.5	1.153	519.7	76.56	92.37	0.9237
C-CDT	0.25	1.953	392.3	128.20	89.89	0.8989
	0.5	1.872	477.1	105.41	91.69	0.9169
	1	1.523	606.0	83.00	93.45	0.9356
	1.5	1.424	703.2	71.52	94.36	0.9436

The Table 5 presents the values of charge transfer resistance (R_t), and double-layer capacitance (C_{dl}) which were derived from Nyquist plots, along with the inhibition efficiency (E_{EIS}) for the corrosion of E24 steel in a 1M HCl solution with varying concentrations of the inhibitor. Notably, the presence of Cedar Tar samples leads to an augmentation in the R_t values while concurrently reducing the C_{dl} values. This decrease in C_{dl} can be attributed to a reduction in the local dielectric constant and/or an increase in the thickness of the electrical double layer [39].

The differences in inhibition efficiency between UNC-CDT and C-CDT can be attributed to their distinct chemical compositions, which impact their adsorption and interaction with the metal surface. UNC-CDT exhibits higher E_{EIS} values than C-CDT at comparable concentrations, suggesting that UNC-CDT may be more effective. However, both inhibitors show improved performance at higher concentrations. The affinity of inhibitor molecules for the metal surface can vary, as can the characteristics of the protective film they form and their influence on electrochemical behavior. These factors collectively contribute to differing inhibitive performances [40].

These changes suggest that Cedar Tar samples adsorb onto the metal surface, forming a protective barrier that inhibits the metal/solution interface [41]. Consequently, the $E_{EIS}\%$

value is expected to increase as the concentration of the inhibitor is increased, as observed from the Tafel polarization method. The EIS spectra of the examined cedar tar were analyzed using the equivalent circuit shown in Figure 6. This circuit represents a single charge transfer reaction and aligns well with the experimental results.

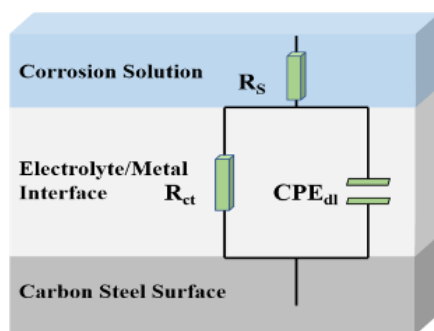


Figure 6. Electrical equivalent circuit.

3.4. Adsorption isotherm

In order to yield valuable insights into the adsorption behavior of the cedar tar samples employed as inhibitors, we can categorize the adsorption of compounds into two primary types: physical adsorption and chemisorption. To delve deeper into the nature and intensity of the adsorption of UNC-CDT and C-CDT on E24 steel, we employed a range of isotherms, including the Temkin, Langmuir, and Frumkin models. Our investigations revealed that the Langmuir isotherm, as defined by Equation 6, played a pivotal role in elucidating this adsorption phenomenon [42–44].

$$\frac{C_{\text{inh}}}{\theta} = \frac{1}{K_{\text{ads}}} + C_{\text{inh}} \quad (6)$$

where C_{inh} is the concentration of inhibitor and K_{ads} the adsorptive equilibrium constant.

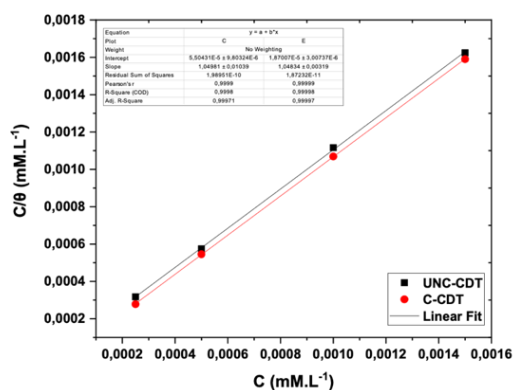


Figure 7. Langmuir adsorption of UNC-CDT and C-CDT on the E24 steel surface in 1 M HCl solution at 293 K.

The Langmuir adsorption isotherm for UNC-CDT and C-CDT is shown in Figure 7. According to this model, it is assumed that the solid surface consists of a fixed number of adsorption sites, each of which securely binds the adsorbed species [8]. The plot in Figure 8 displays a straight line with a slope approximating 1, signifying that the adsorption of UNC-CDT and C-CDT at the E24 steel/acidic solution interface adheres to Langmuir's adsorption isotherm model.

The values of K_{ads} obtained from the reciprocal of the intercept of the Langmuir isotherm are listed in Table 6, along with the values of the Gibbs free energy of adsorption calculated from Equation 7: ΔG_{ads}^0 [8–12].

$$K_{\text{ads}} = \frac{1}{55.5} \exp\left(-\frac{\Delta G_{\text{ads}}^0}{RT}\right) \quad (7)$$

where R is the universal gas constant (kJ/mol·K), T the thermodynamic temperature (K), and the value of 55.5 is the water concentration in acidic solution (mol/L).

The ΔG_{ads}^0 value offers insights into the nature of the interaction between inhibitor molecules and the metallic surface. Typically, energy values of ΔG_{ads}^0 around -20 kJ/mol or less negative are indicative of electrostatic interactions (physisorption) between positively charged inhibitors and the metal surface. Conversely, when ΔG_{ads}^0 values reach approximately -40 kJ/mol or higher, it suggests electron transfer or sharing between the inhibitor molecules and the metal surface, culminating in the formation of a coordinated covalent bond (chemisorption) [34].

Table 6. Thermodynamic parameters for the adsorption of UNC-CDT and CDT in 1 M HCl on the E24 steel at 293 K.

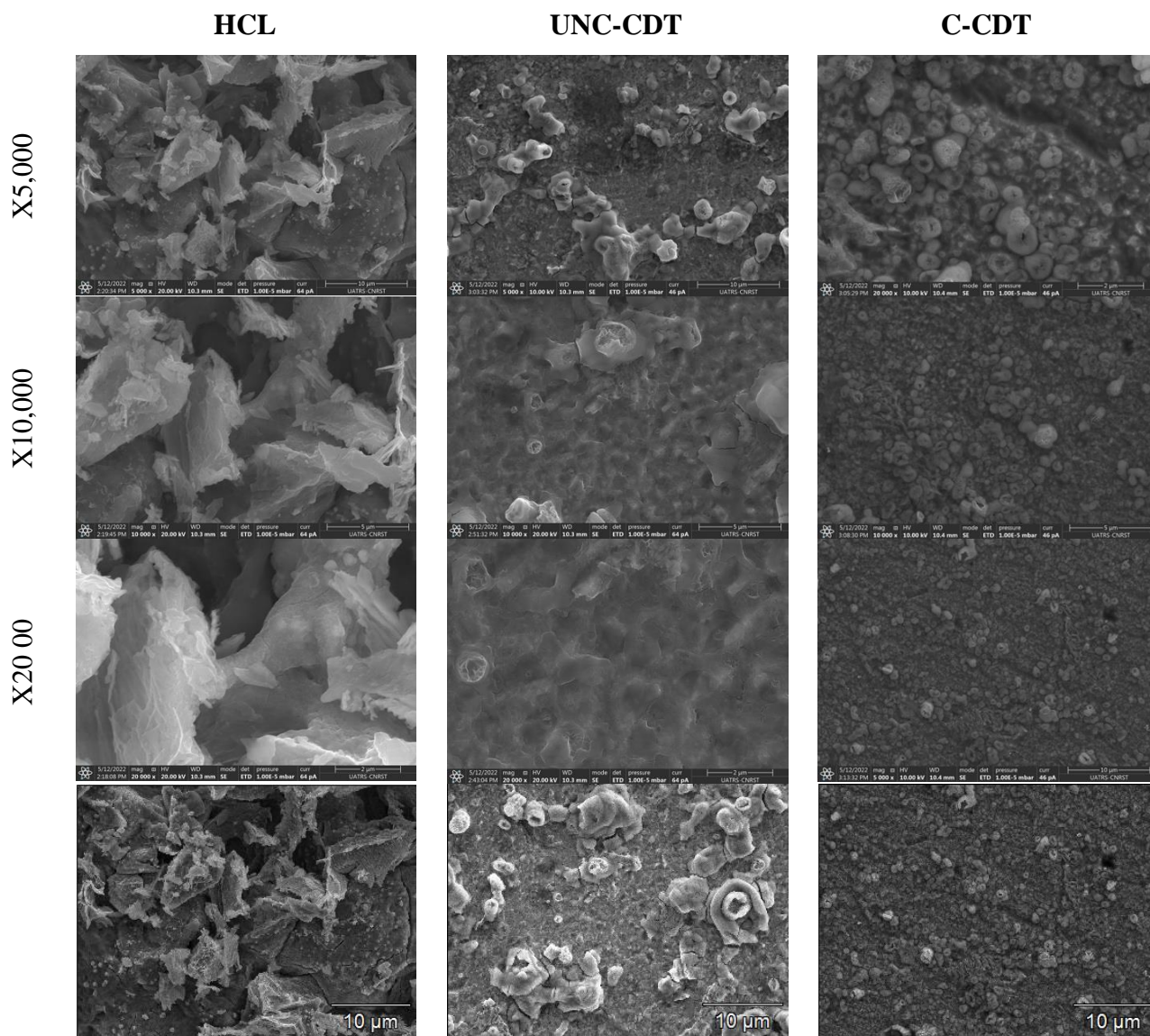
Inhibitor	K , mol ⁻¹ ·L	R^2	ΔG_{ads}^0 kJ/mol
UNC-CDT	$0.181 \cdot 10^5$	0.99	-34.27
C-CDT	$0.535 \cdot 10^5$	0.99	-36.94

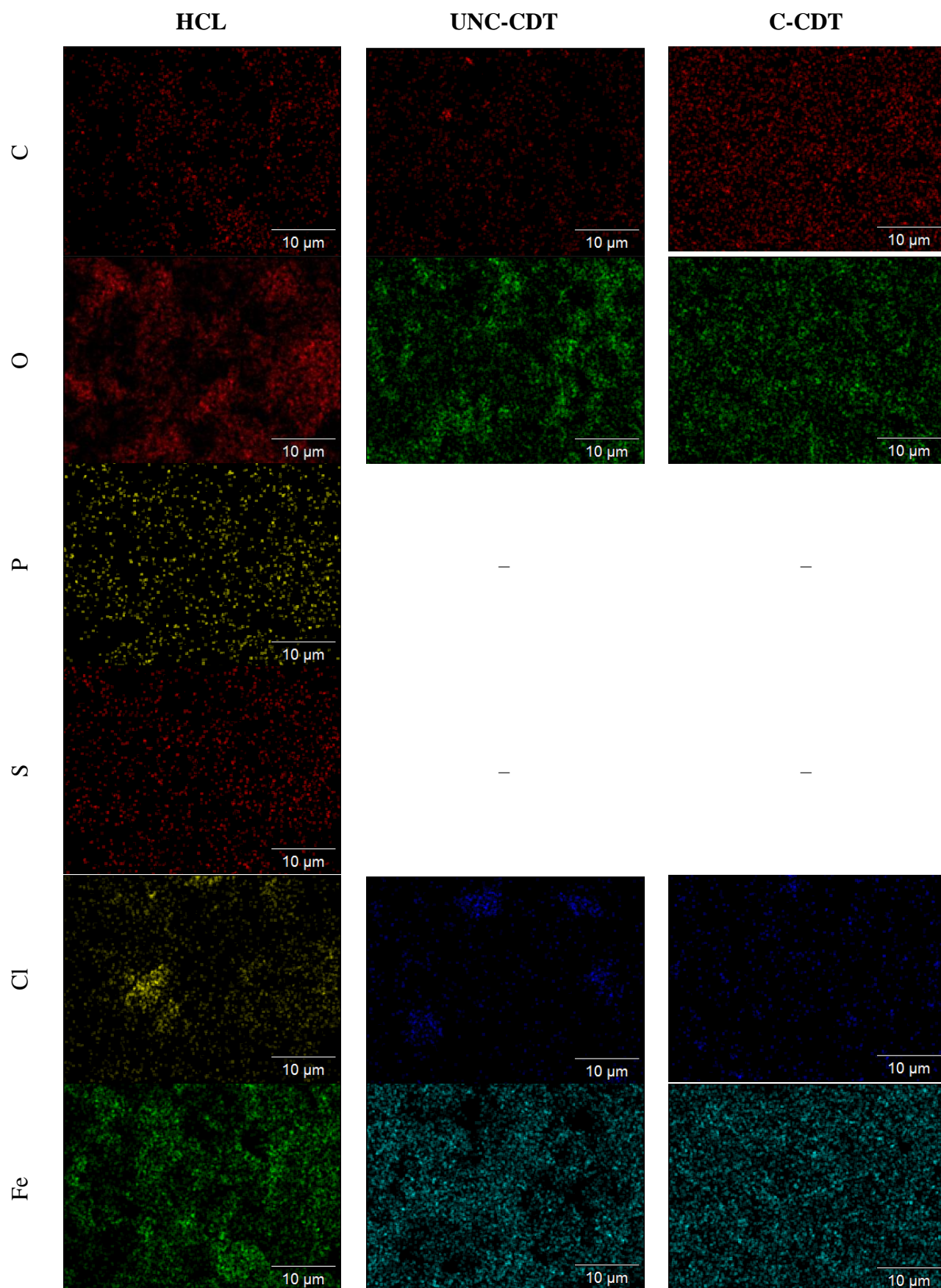
The data in Table 6 revealed that the Cedar Tar samples were rapidly and strongly adsorbed onto the E24 surface. The adsorption of both UNC-CDT and C-CDT on the E24 steel surface follows both physical adsorption (physisorption) and chemical adsorption (chemisorption) modes, forming a coordinate bond between the investigated inhibitor molecules and the surrounding d -orbitals of the E24 steel surface [45].

3.5. Surface morphology

The Figure 8 depicts the micrographs of E24 steel samples along with the corresponding EDX spectra to determine the elemental composition (%) on the surface. These analyses were conducted after a 24-hour immersion in the test solution of 1 M HCl, both with and without 1.5 g/L of UNC-CDT and C-CDT inhibitors.

In Figure 8, the surface of E24 steel is shown to have experienced severe corrosion attack when immersed in 1 M HCl for 24 h. However, when cedar tar samples were added to the test solution, a remarkable change was observed on the E24 steel surface. The specimen surface became smoother, as depicted in the figure. It is assumed that the formation of a protective layer is randomly distributed on the entire surface of E24 steel. This protective layer is believed to be a result of the adsorption of active molecules present in the cedar tar onto the E24 steel surface, effectively incorporating into the passive film and blocking the active sites on the E24 steel surface [4, 45, 46].





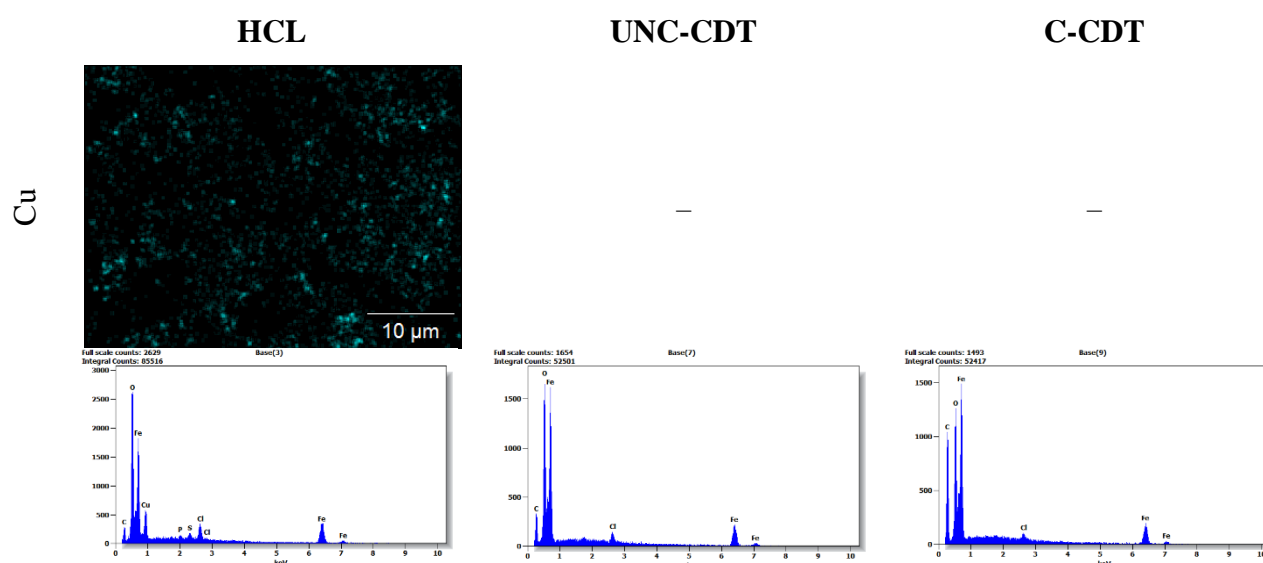


Figure 8. SEM micrographs and EDX spectra of E24 steel surface after 24 h of immersion in 1 M HCl and with and without 1.5 g/L UNC-CDT and C-CDT samples at 25°C.

The results of the element weight% in the surface composition of E24 after immersion in 1 M HCl, both without and with UNC-CDT and C-CDT inhibitors tested at 25°C, are presented in Table 7.

Table 7. Surface composition (wt%) of E24 steel after immersion in 1 M HCl without and with 1.5 g/L inhibitors tested at 25°C.

Element (wt%)	1 M HCl	UNC-CDT	C-CDT
C	1.77	3.08	9.10
O	18.01	15.52	11.89
P	0.62	0.00	0.00
S	1.36	0.00	0.00
Cl	4.18	2.53	1.60
Fe	60.05	78.87	77.41
Cu	14.01	0.00	0.00

It is evident that the element weight % in the surface composition of E24 has been reduced in the presence of both UNC-CDT and C-CDT inhibitors, and some elements have disappeared due to the overlying inhibitor film [47]. The percentage of carbon has increased, going from 1.77% to 3.08% for UNC-CDT and significantly to 9.10% for C-CDT. This notable increase in carbon content can be attributed to a layer formed due to the adsorption of various chemical constituents present in Cedar tar samples onto the metal surface [48]. The increase in iron content after the addition of corrosion inhibitors is due to the protective film formed by the inhibitors, shielding the iron from corrosion and reducing its dissolution

or oxidation. Additionally, the presence of inhibitors results in a decrease in oxygen (O) content, indicating reduced oxide formation and hindered oxidation processes. These results corroborate the conclusions drawn from electrochemical measurements, indicating the presence of a surface film that hinders the dissolution of the metal. As a result, this film effectively delays the occurrence of the hydrogen evolution reaction.

Furthermore, the chemical composition analysis of UNC-CDT and CDT revealed an abundance of compounds with varying low percentages. This rich chemical diversity points to the possibility that the corrosion may be influenced by the effects of multiple compounds. To gain a comprehensive understanding, further studies are essential to determine the specific elements that were adsorbed onto the surface of E24.

4. Conclusions

The objective of this study was to evaluate the efficacy of cedar tar as an environmentally friendly corrosion inhibitor for E24 steel in a 1 M HCl solution. Both UNC-CDT and C-CDT were found to be predominantly composed of epi- β -Caryophyllene, α -himachalene, (*E*)-atlantone, γ -himalachene, and 4-acetyl-1-methylcyclohexene, which are present in varying proportions in each sample, the variations in the chemical composition and the presence or absence of certain elements between UNC-CDT and C-CDT, along with the differing percentages of key compounds, contribute to the differences in inhibition efficiency observed in this study. The unique composition of each inhibitor, including the presence of specific elements or compounds, can influence their inhibitive performance. These disparities in composition can impact the affinity of the inhibitors for the metal surface, their ability to form protective films and their overall inhibitive effectiveness. The results from Tafel polarization measurements indicate that both UNC-CDT and C-CDT function as mixed-type inhibitors. As the concentration of CDT increases, its inhibitive properties improve significantly, reaching an impressive 93.09% and 95.51% at 1.5 g/L for UNC-CDT and C-CDT, respectively.

Furthermore, the study reveals that higher inhibitor concentrations lead to an augmentation of charge transfer resistance while concurrently causing a reduction in double-layer capacitance values. These observed alterations strongly imply the formation of protective layers on the E24 steel surface. These layers act as a robust shield, effectively mitigating rapid degradation and corrosion when exposed to an HCl solution. The Langmuir adsorption isotherm model further supports the strong adsorption characteristics of UNC-CDT and C-CDT inhibitors on the steel surface. The electrochemical tests conclusively demonstrate the remarkable efficiency of cedar tar as a sustainable corrosion inhibitor for E24 steel in acidic environments, highlighting its potential for practical applications in corrosion protection.

Acknowledgments

The authors would like to express their gratitude to the Forest Research Center – Rabat and its team, as well as the National Center for Scientific and Technical Research (CNRST) of

Morocco for providing the technical facilities of the UATS Division. Special thanks are also extended to Dr. Khadija El Maalam from the Moroccan Foundation for Advanced Science, Innovation, and Research (MAScIR) Institute for conducting the chemical composition analysis.

References

1. J. Wen, X. Zhang, Y. Liu, B. Shang, J. He and L. Li, Exploration of Imidazol-4-Methylimine Thiourea as Effective Corrosion Inhibitor for Mild Steel in Hydrochloric Medium: Experimental and Theoretical Studies, *Colloids Surf., A*, 2023, **674**, 131895. doi: [10.1016/j.colsurfa.2023.131895](https://doi.org/10.1016/j.colsurfa.2023.131895)
2. H. Elmsellem, H. Bendaha, A. Aouniti, A. Chetouani, M. Mimouni and A. Bouyanzer, Comparative study of the inhibition of extracts from the peel and seeds of Citrus Aurantium against the corrosion of steel in molar HCl solution, *Moroccan J. Chem.*, 2014, **2**, 1–9. doi: [10.13140/RG.2.1.4603.5360](https://doi.org/10.13140/RG.2.1.4603.5360)
3. C. Zhang, K. Yamanaka, H. Bian and A. Chiba, Corrosion-resistant carbide-reinforced martensitic steel by Cu modification, *npj Mater. Degrad.*, 2019, **3**, 30. doi: [10.1038/s41529-019-0092-3](https://doi.org/10.1038/s41529-019-0092-3)
4. K. Cisse, D. Gassama, A. Thiam, E.H.B. Ndiaye, M.T. Gueye and M. Fall, Comparative Study of S235 Steel Corrosion Inhibition by Eucalyptus camaldulensis and Cyperus rotundus Essential Oils in Hydrochloric Acid Solution, *Am. J. Phys. Chem.*, 2021, **10**, 6–15. doi: [10.11648/j.ajpc.20211001.12](https://doi.org/10.11648/j.ajpc.20211001.12)
5. S. Cherrad, I. Jaouadi, Y. El Aoufir, M. Tiskar, B. Satrani, M. Ghanmi, A. Guenbour, and A. Chaouch, Unveiling corrosion inhibition properties of the cupressus arizonica leaves essential oil for carbon steel in 1.0 M HCl, *Int. J. Corros. Scale Inhib.*, 2020, **9**, no. 2, 607–622. doi: [10.17675/2305-6894-2020-9-2-15](https://doi.org/10.17675/2305-6894-2020-9-2-15)
6. M. Znini, Application of Essential Oils as green corrosion inhibitors for metals and alloys in different aggressive mediums - A review-, *Arabian Journal of Medicinal and Aromatic Plants*, 2019, **5**, 1–34. doi: [10.48347/IMIST.PRSM/ajmap-v5i3.18664](https://doi.org/10.48347/IMIST.PRSM/ajmap-v5i3.18664)
7. Y.P. Asmara, T. Kurniawan, A.G.E. Sutjipto and J. Jafar, Application of plants extracts as green corrosion inhibitors for steel in concrete – A review, *Indonesian J. Sci. Technol.*, 2018, **3**, 158–170. doi: [10.17509/ijost.v3i2.12760](https://doi.org/10.17509/ijost.v3i2.12760)
8. I. Jaouadi, S. Cherrad, M. Tiskar, M. Tabyaoui, M. Ghanmi, B. Satrani and A. Chaouch, Wood tar essential oil from cedrus atlantica of morocco (Middle atlas) as a green corrosion inhibitor for mild steel in 1 M hydrochloric acid solution, *Int. J. Corros. Scale Inhib.*, 2020, **9**, no. 1, 265–283. doi: [10.17675/2305-6894-2020-9-1-17](https://doi.org/10.17675/2305-6894-2020-9-1-17)

-
9. S. Burri, M. Alifriqui, S.-S. Bun, C. Cenzon-Salvayre, I.H. Cigerci, A. Cloarec, R. Corbineau, D. Robles, A. Angelina, A. Durand, M. El Jemli, X. Fernandez, D. Genin, M. Ghanmi, M. Konuk, S. Le Maguer, R. Liman, M. Ilias, A. Mazuy, D. Ollivier, E. Ollivier, M. Regert, B. Satrani and Y. Kaan, Des ressources naturelles à la santé : Approche interdisciplinaire de la production des goudrons de conifères et de leur usage médicinal en Méditerranée sur la longue durée, *Les Nouvelles de l'archéologie*, 2018, **152**, 62–69. doi: [10.4000/nda.4267](https://doi.org/10.4000/nda.4267)
 10. O. Ninich, A. Et-tahir, K. Kettani, M. Ghanmi, J. Aoujdad, S. El Antry, M. Ouajdi and B. Satrani, Plant sources, techniques of production and uses of tar : A review, *J. Ethnopharmacol.*, 2022, **285**, 114889. doi: [10.1016/j.jep.2021.114889](https://doi.org/10.1016/j.jep.2021.114889)
 11. O. Ninich, A. Ettahir, K. Kettani, M. Ghanmi, J. Aoujdad, S. El- Antry, M. Ouajdi, S. Burri and B. Satrani, Moroccans' ethnobotanical knowledge about medicinal tar, *Trop. J. Nat. Prod. Res.*, 2022, **6**, 317–329. <https://shs.hal.science/halshs-03845067>
 12. A. Turkustani, N.M. Gumgumji and A.S. Al Hajar, Olea europaea Subsp. Cuspidata Wood Tar Oil as Anticorrosion for Mild steel in Acidic Media, *Asian J. Chem.*, 2019, **31**, 1558–1564. doi: [10.14233/ajchem.2019.21977](https://doi.org/10.14233/ajchem.2019.21977)
 13. A. Aiboud, A. Moussaif, N. El Abbadi, A. Ettabia, A. El Hessni, A. Ouichou, M. Chakit and A. Mesfioui, In Vitro Antidermatophytic Activity of Allium Sativum L, Nicotina Tabacum and Cade Oil Against Trichophyton Rubrum, *World J. Pharm. Res.*, 2015, **4**, 414–423.
 14. A. Aiboud, Caractérisation phytochimique et étude de l'action antidermatophytique in vitro et in vivo du goudron de Cedrus atlantica, Nicotiana tabacum et Allium sativum L, Université Ibn Tofail, 2016.
 15. I. Skanderi and O. Chouitah, Chemical Characterization and Antioxidant Activity of Cedrus atlantica Manetti Tar (Atlas Cedar Tar), *Fr.-Ukr. J. Chem.*, 2020, **8**, 244–255. doi: [10.17721/fujcv8i2p244-255](https://doi.org/10.17721/fujcv8i2p244-255)
 16. K. Tassaoui, M. Damej, A. Molhi, A. Berisha, M. Errili, S. Ksama, V. Mehmeti, S. El Hajjaji and M. Benmessaoud, Contribution to the corrosion inhibition of Cu–30Ni copper–nickel alloy by 3-amino-1,2,4-triazole-5-thiol (ATT) in 3% NaCl solution. Experimental and theoretical study (DFT, MC and MD), *Int. J. Corros. Scale Inhib.*, 2022, **11**, no. 1, 221–244. doi: [10.17675/2305-6894-2022-11-1-12](https://doi.org/10.17675/2305-6894-2022-11-1-12)
 17. K. Tassaoui, A. Al-shami, M. Damej, A. Molhi, O. Mounkachi and M. Benmessaoud, Contribution to the corrosion inhibitors of copper-nickel (Cu-30Ni) in 3 % NaCl solution by two new molecules of triazole : Electrochemical and theoretical studies, *J. Mol. Struct.*, 2023, **1291**, 135836. doi: [10.1016/j.molstruc.2023.135836](https://doi.org/10.1016/j.molstruc.2023.135836)
 18. M. Damej, S. Skal, J. Aslam, M. Zouarhi, H. Erramli, A.A. Alrashdi, H.S. Lee, Y. El aoufir and H. Lgaz, An environmentally friendly formulation based on Cannabis sativa L. seed oil for corrosion inhibition of E24 steel in HCl medium: Experimental and theoretical study, *Colloids Surf., A*, 2022, **643**, 128745. doi: [10.1016/j.colsurfa.2022.128745](https://doi.org/10.1016/j.colsurfa.2022.128745)

19. Y. Kurt, M.S. Kaçar and K. Isik, Traditional tar production from *Cedrus libani* A. Rich on the Taurus Mountains in southern Turkey, *Econ. Bot.*, 2008, **62**, 615–620.
20. L. Bailly, Caractérisation moléculaire et isotopique de goudrons et résines archéologiques dérivés de conifères en contexte maritime, Université de Strasbourg, 2015.
21. M. Rageot, Les substances naturelles en Méditerranée nord-occidentale (VIe-Ier millénaire BCE): chimie et archéologie des matériaux exploités leurs propriétés adhésives et hydrophobes, Université Nice Sophia Antipolis, 2015.
22. A. El Abid, Bilan Des Recherches Au Maroc en matière d'exploitation et valorisation de cedre, *Ann. Rech. For. Maroc*, 1994, **27**, 627–637.
23. A.K. Pekgözlü, S. Kuştaş, B. Mercan and A. Biçer, Analiza kemijskog sastava katrana od libanonskog cedra, *Drvna Ind.*, 2017, **68**, 107–112. doi: [10.5552/drind.2017.1607](https://doi.org/10.5552/drind.2017.1607)
24. J.C. Chalchat, R.P. Garry, A. Miehet and B. Benjlali, Essential oil components in sawdust of *Cedrus atlantica* from Morocco, *J. Essent. Oil Res.*, 1994, **6**, 323–325. doi: [10.1080/10412905.1994.9698386](https://doi.org/10.1080/10412905.1994.9698386)
25. T.D. Manh, T.L. Huynh, B.V. Thi, S. Lee, J. Yi and N.N. Dang, Corrosion Inhibition of Mild Steel in Hydrochloric Acid Environments Containing *Sonneratia caseolaris* Leaf Extract, *ACS Omega*, 2022, **7**, 8874–8886. doi: [10.1021/acsomega.1c07237](https://doi.org/10.1021/acsomega.1c07237)
26. R. Karthikaiselvi and S. Subhashini, Study of adsorption properties and inhibition of mild steel corrosion in hydrochloric acid media by water soluble composite poly (vinyl alcohol-o-methoxy aniline), *J. Assoc. Arab Univ. Basic Appl. Sci.*, 2014, **16**, 74–82. doi: [10.1016/j.jaubas.2013.06.002](https://doi.org/10.1016/j.jaubas.2013.06.002)
27. N. Labjar, F. Bentiss, M. Lebrini, C. Jama and S. El Hajjaji, Study of temperature effect on the corrosion inhibition of C38 carbon steel using amino-tris(methylenephosphonic) acid in hydrochloric acid solution, *Int. J. Corros.*, 2011, **2011**, 548528. doi: [10.1155/2011/548528](https://doi.org/10.1155/2011/548528)
28. J. Bhawsar, P.K. Jain and P. Jain, Experimental and computational studies of *Nicotiana tabacum* leaves extract as green corrosion inhibitor for mild steel in acidic medium, *Alexandria Eng. J.*, 2015, **54**, 769–775. doi: [10.1016/j.aej.2015.03.022](https://doi.org/10.1016/j.aej.2015.03.022)
29. A. Zomorodian and A. Behnood, Review of Corrosion Inhibitors in Reinforced Concrete: Conventional and Green Materials, *Buildings*, 2023, **13**, 1170. doi: [10.3390/buildings13051170](https://doi.org/10.3390/buildings13051170)
30. B.R. Fazal, T. Becker, B. Kinsella and K. Lepkova, A review of plant extracts as green corrosion inhibitors for CO₂ corrosion of carbon steel, *npj Mater. Degrad.*, 2022, **6**, 5. doi: [10.1038/s41529-021-00201-5](https://doi.org/10.1038/s41529-021-00201-5)
31. O. Boumediene, M. Tourabi, O. Benali, C. Selles, M. Traisnel, C. Jama, F. Bentiss and R. Salghif, Experimental investigation on the corrosion inhibition characteristics of mild steel by 5-(2-hydroxyphenyl)-1,3,4-oxadiazole-2-thiol in hydrochloric acid medium, *J. Mater. Environ. Sci.*, 2016, **7**, 2971–2988.

-
32. A.Y. Musa, A.A.H. Kadhum, A.B. Mohamad, M.S. Takriff, A.R. Daud and S.K. Kamarudin, On the inhibition of mild steel corrosion by 4-amino-5-phenyl-4H-1,2,4-triazole-3-thiol, *Corros. Sci.*, 2010, **52**, 526–533. doi: [10.1016/J.CORSCI.2009.10.009](https://doi.org/10.1016/J.CORSCI.2009.10.009)
 33. Y. Aouine, M. Sfaira, M. Ebn Touhami, A. Alami, B. Hammouti, M. Elbakri, A. El Hallaoui and R. Tourir, Temperature and time investigations on the adsorption behavior of isoindoline, tetrazole and isoindoline-tetrazole on corrosion of mild steel in acidic medium, *Int. J. Electrochem. Sci.*, 2012, **7**, 5400–5419. doi: [10.1016/s1452-3981\(23\)19630-1](https://doi.org/10.1016/s1452-3981(23)19630-1)
 34. L. Chen, D. Lu and Y. Zhang, Organic Compounds as Corrosion Inhibitors for Carbon Steel in HCl Solution: A Comprehensive Review, *Materials*, 2022, **15**, 2–59. doi: [10.3390/ma15062023](https://doi.org/10.3390/ma15062023)
 35. K. Alaoui, Y. El Kacimi, M. Galai, R. Tourir, K. Dahmani, A. Harfi and M. Ebn Touhami, Anti-corrosive properties of polyvinyl-alcohol for carbon steel in hydrochloric acid media: Electrochemical and thermodynamic investigation, *J. Mater. Environ. Sci.*, 2016, **7**, 2389–2403.
 36. M. Husaini, U. Yunusa, H.A. Ibrahim, B. Usman and B. Ibrahim, Corrosion inhibition of aluminium in phosphoric acid solution using glutaraldehyde as inhibitor, *Al. J. Chem. Eng.*, 2020, **01**, 12–21. doi: [10.5281/zenodo.3986577](https://doi.org/10.5281/zenodo.3986577)
 37. M. Boudalia, R.M. Fernández-Domene, M. Tabyaoui, A. Bellaouchou, A. Guenbour, and J. García-Antón, Green approach to corrosion inhibition of stainless steel in phosphoric acid of Artemesia herba albamedium using plant extract, *J. Mater. Res. Technol.*, 2019, **8**, 5763–5773. doi: [10.1016/j.jmrt.2019.09.045](https://doi.org/10.1016/j.jmrt.2019.09.045)
 38. L. Afia, R. Salghi, L. Bammou, E. Bazzi, B. Hammouti, L. Bazzi and A. Bouyanzer, Anti-corrosive properties of Argan oil on C38 steel in molar HCl solution, *J. Saudi Chem. Soc.*, 2014, **18**, 19–25. doi: [10.1016/j.jsccs.2011.05.008](https://doi.org/10.1016/j.jsccs.2011.05.008)
 39. S. John, R. Jeevana, K.K. Aravindakshan and A. Joseph, Corrosion inhibition of mild steel by N(4)-substituted thiosemicarbazone in hydrochloric acid media, *Egypt. J. Pet.*, 2017, **26**, 405–412. doi: [10.1016/j.ejpe.2016.05.012](https://doi.org/10.1016/j.ejpe.2016.05.012)
 40. A. Singh, E.E. Ebenso and M.A. Quraishi, Corrosion inhibition of carbon steel in HCl solution by some plant extracts, *Int. J. Corros.*, 2012, **2012**, 897430. doi: [10.1155/2012/897430](https://doi.org/10.1155/2012/897430)
 41. M.T. Alhaffar, S.A. Umoren, I.B. Obot and S.A. Ali, Isoxazolidine derivatives as corrosion inhibitors for low carbon steel in HCl solution: Experimental, theoretical and effect of KI studies, *RSC Advances*, 2018, **8**, 1764–1777. doi: [10.1039/c7ra11549k](https://doi.org/10.1039/c7ra11549k)
 42. J.S. Piccin, G.L. Dotto and L.A.A. Pinto, Adsorption isotherms and thermochemical data of FDandC RED N° 40 Binding by chitosan, *Braz. J. Chem. Eng.*, 2011, **28**, 295–304. doi: [10.1590/S0104-66322011000200014](https://doi.org/10.1590/S0104-66322011000200014)
 43. M.M. Kamel, A.A.S. Fouda, S.M. Rashwan and O. Abdelkader, Paprika extract: a green inhibitor for mitigating carbon steel disintegration in 1 M HCl pickling solution, *Green Chem. Lett. Rev.*, 2021, **14**, 600–611. doi: [10.1080/17518253.2021.1985173](https://doi.org/10.1080/17518253.2021.1985173)

-
44. J.T. Nwabanne and V.N. Okafor, Adsorption and Thermodynamics Study of the Inhibition of Corrosion of Mild Steel in H₂SO₄ Medium Using *Vernonia amygdalina*, *J. Miner. Mater. Charact. Eng.*, 2012, **11**, 885–890. doi: [10.4236/jmmce.2012.119083](https://doi.org/10.4236/jmmce.2012.119083)
45. M. Damej, S. Kaya, B. EL Ibrahim, H.S. Lee, A. Molhi, G. Serdaroglu, M. Benmessaoud, I.H. Ali, S. EL Hajjaji and H. Lgaz, The corrosion inhibition and adsorption behavior of mercaptobenzimidazole and bis-mercaptobenzimidazole on carbon steel in 1.0 M HCl: Experimental and computational insights, *Surf. Interfaces*, 2021, **24**, 101095. doi: [10.1016/j.surfin.2021.101095](https://doi.org/10.1016/j.surfin.2021.101095)
46. A. Abdeslam, M. Mounir, Z. Mohamed, L. Zouhair and A. Mohamed, Experimental and theoretical study on corrosion inhibition of new synthesized menthone derivatives (Menthopyrazole compounds) for mild steel in 1 M HCl solution, *Mediterr. J. Chem.*, 2020, **10**, 62–76. doi: [10.13171/mjc101020291189aa](https://doi.org/10.13171/mjc101020291189aa)
47. Ya.G. Avdeev, T.A. Nenasheva, L.V. Frolova, A.I. Marshakov and Yu.I. Kuznetsov, Cathodic reduction of hydrogen on low-carbon steel in solutions of mineral acids containing nitrogen-containing organic compounds, *Int. J. Corros. Scale Inhib.*, 2021, **10**, 262–283. doi: [10.17675/2305-6894-2021-10-1-15](https://doi.org/10.17675/2305-6894-2021-10-1-15)
48. A.A. Al-Amiery, W.K. Al-Azzawi and W.N.R.W. Isahak, Isatin Schiff base is an effective corrosion inhibitor for mild steel in hydrochloric acid solution: gravimetical, electrochemical, and computational investigation, *Sci. Rep.*, 2022, **12**, 17773. doi: [10.1038/s41598-022-22611-4](https://doi.org/10.1038/s41598-022-22611-4)

